

# Structural and Energetic Determinants of Thermal Stability and Hierarchical Unfolding Pathways of Hyperthermophilic Proteins, Sac7d and Sso7d

U. Deva Priyakumar,\* S. Ramakrishna, K. R. Nagarjuna, and S. Karunakar Reddy

Center for Computational Natural Sciences and Bioinformatics, International Institute of Information Technology, Hyderabad 500 032, India

Received: September 22, 2009; Revised Manuscript Received: November 13, 2009

Identification of the structural and energetic determinants responsible for enhancing the stability of proteins is crucial. Hyperthermophilic proteins are naturally occurring proteins that exhibit high thermal stability and are good candidates for the investigation and understanding of structure–stability relationships. Sac7d from *Sulfolobus acidocaldarius* and Sso7d from *Sulfolobus solfataricus* are two homologous hyperthermophilic proteins that were shown to be quite stable at high temperatures. Molecular dynamics simulations at the nanosecond time scale at different temperatures were performed to examine the factors affecting their stability. The three-dimensional structures of these proteins were observed to be similar to the experimental structure at 300 and 360 K but were found to undergo denaturation at 500 K. Both proteins exhibit similar unfolding pathways that correlates well with the calculated intermolecular interaction energies. The differential dynamic behaviors of these molecules at different temperatures were examined. Structural and energetic analysis of the contributions of salt bridges indicates a stabilizing effect at higher temperatures. However, the lifetimes of the salt bridges were found to be quite short, and several new salt bridges formed at 500 K supporting previous studies that the desolvation penalty due to the formation of salt bridges decreases at elevated temperatures. Hydrophobic interactions, which decrease with increase in temperature, were also found to be crucial in the stability of these proteins. Overall, the study shows that a balance among the salt bridge interactions, hydrophobic interactions, and solvent properties is primarily responsible for the high thermal stability of this class of proteins.

## Introduction

Extremophiles are microorganisms that are capable of adapting to extreme physiological conditions. Some of them include thermophiles and hyperthermophiles, acidophiles, alkaliphiles, halophiles, and psychrophiles, which thrive at high temperatures, low pH, high pH, high concentrations of salt, and freezing temperatures, respectively.<sup>1,2</sup> Hyperthermophiles are examples of such species that display optimum growth at temperatures in the range of 80–100 °C.<sup>3–7</sup> These microorganisms have developed heat-resistant proteins—thermophilic and hyperthermophilic proteins—which are stable at these temperatures and are capable of performing their biological functions. Certain hyperthermophilic proteins are also capable of binding to DNA and RNA nonspecifically and assisting the nucleic acid duplexes to resist denaturation at temperatures up to 90 °C, exhibiting histone like functions.<sup>3,8,9</sup> Remarkably, these proteins are very similar to their mesophilic homologues in terms of both their sequence and the three-dimensional structure, but the mesophilic proteins are stable only at normal conditions. Several of the thermophilic proteins whose structures are known were found to be highly superimposable onto their mesophilic analogues (for example, ribonuclease H1 enzyme from *T. thermophilus* and the ribonuclease H1 from *E. coli*).<sup>10,11</sup> The structural similarity between the hyperthermophilic proteins and their mesophilic analogues, despite having completely different thermal profiles, makes the identification of the determinants responsible for the hyperthermal stability more difficult. In addition to their role in biological functions, thermal stability

of proteins is also appealing in industrial biocatalysis since thermophilic enzyme assisted reactions can be carried out at higher temperatures which is useful in increasing the rate, yield, etc.<sup>5,12–14</sup> Hence, atomistic investigations of the structural, energetic, and dynamic properties of these proteins are crucial for the understanding of the factors involved in the stabilization of proteins in general.

Several studies have examined the structural differences between hyperthermophilic and mesophilic proteins based on the available experimental structures. Some of the factors that have been shown to be more prevalent in hyperthermophilic proteins compared to the mesophilic ones are the increased number of salt bridges, the presence of a strong hydrophobic core, high compactness of the structures, and reduced number of cavities, among others.<sup>15–24</sup> The role of electrostatic interactions arising from salt bridges has been a subject of controversy. Studies have suggested salt bridges to have a stabilizing effect, no effect, and destabilizing effect on the overall stability of these proteins.<sup>25–29</sup> The significant desolvation penalty due to the association of charged residues during the formation of a salt bridge was suggested to have an unfavorable effect on the stabilization of thermophilic proteins. However, experimental and computational studies have shown that the desolvation penalty decreases with increase in temperature and are capable of stabilizing the three-dimensional structures at elevated temperatures.<sup>26,28</sup> Similarly, the role of hydrophobic interactions on the thermal stability of proteins has been debated over the years.<sup>29–32</sup> It has been shown that the stabilizing contribution from a single hydrophobic contact remains unchanged compared to other types of interactions.<sup>29</sup>

\* Corresponding author. E-mail: deva@iiit.ac.in. Phone: +91-40-6653 1161. Fax: +91-40-6653 1413.

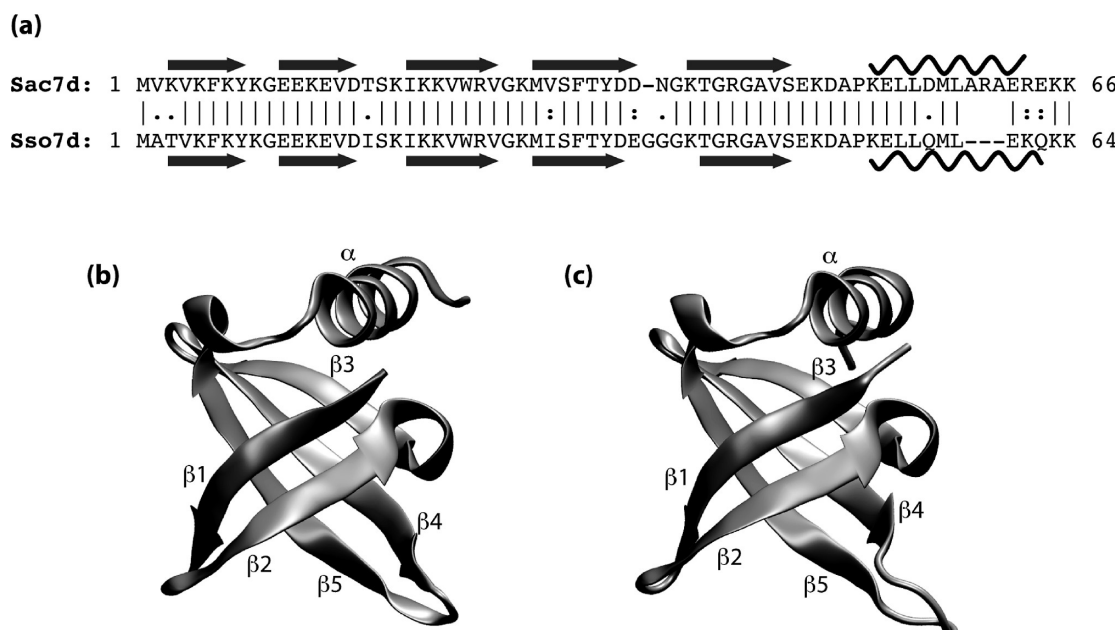


**Figure 1.** (a) Primary sequence of Sac7d and Sso7d proteins along with sequence alignment results. The secondary structure elements,  $\beta$  strands and  $\alpha$  helices, are denoted by gray arrows and wavy lines, respectively. The three-dimensional structures of Sac7d (b) and Sso7d (c) generated using the VMD program.<sup>58</sup> Both proteins are depicted in similar orientations; alignment was done using the SuperPose server.<sup>66</sup>

Molecular dynamics (MD) simulations have been indispensable in understanding structure function relationships of biological macromolecules and are capable of providing atomic level details of their structures and dynamics.<sup>33,34</sup> The relative stabilities of thermophilic and hyperthermophilic proteins have been studied using MD simulations performed at different temperatures.<sup>35–40</sup> A study by de Bakker et al. based on 1 ns MD simulation of Sac7d protein examined the factors responsible for thermal stability.<sup>35</sup> However, the protein did not undergo denaturation even at 550 K within 1 ns of the simulation. The authors suggested that the possible reasons for the in silico stability might be due to the cutoff scheme, force field parameters, and particle–particle particle–mesh method used in the simulations. The stability and unfolding pathways of mesophilic proteins have also been studied based on MD simulations done at higher temperatures.<sup>41,42</sup>

In the current paper, two hyperthermophilic proteins, Sac7d from *Sulfolobus acidocaldarius* and Sso7d from *Sulfolobus solfataricus*, whose melting temperature was shown to be above 90 °C,<sup>43–45</sup> are studied. Sac7d and Sso7d are homologous proteins, which are similar at primary, secondary, and tertiary structural levels (Figure 1). Global alignment of the two sequences using the Needleman–Wunsch algorithm<sup>46</sup> shows about 87% similarity. Both the structures consist of a double-stranded β-sheet packed onto a triple-stranded β-sheet capped by a C-terminal α-helix, and the three-dimensional structures are highly superimposable (Figure 1). We attempt to answer the following questions by examining the structural, dynamic, and energetic aspects: (a) Are the methodology adopted and the force field used capable of accurately representing the thermal stability of these proteins? (b) What are the structural and energetic features responsible for the thermal stability? (c) How do the salt bridges, hydrophobic interactions, and solvation properties affect the thermal stability? (d) How do the dynamic properties alter with respect to high temperature? (e) Do the proteins undergo unfolding at temperatures higher than the organisms' physiological growth temperature? MD simulations were performed under explicit solvent conditions at three different temperatures to answer the above points.

### Computational Details

**MD Simulations.** The MD simulations reported in the present study were performed using the CHARMM program<sup>47</sup> applying the all-atom protein CHARMM22 force field<sup>48</sup> along with CMAP correction.<sup>49</sup> The crystal structures of Sac7d and Sso7d proteins were obtained from the published data,<sup>50,51</sup> to which hydrogen atoms were added using the HBUILD utility in CHARMM. The structures were then submerged into a truncated octahedron water box, which was previously equilibrated at room temperature. The size of the water box was chosen such that the distance from any non-hydrogen atom of the protein to the boundary of the box was at least 9 Å. On the basis of a distance cut off of 2.4 Å between the non-hydrogen atoms of the protein and the oxygen of water, overlapping water molecules were eliminated. A modified TIP3P water model was used for the explicit solvation in all the simulations.<sup>52</sup> In the resultant water box containing the protein, chloride ions were added to maintain electrical neutrality. The solvated box used for simulations contained a total of 18 048 atoms including 5663 water molecules and 5 and 6 chloride ions in Sac7 and Sso7d, respectively. During the energy minimizations and MD simulations, the periodic boundary condition was implemented via the CRYSTAL module<sup>53</sup> built in CHARMM. Initially, the systems were subjected to 1000-step adopted basis Newton–Raphson minimization, followed by a 100 ps MD simulation at the NVT ensemble at 300 K. During the energy minimization and the MD simulation, the non-hydrogen atoms of the protein were restrained using mass weighted harmonic constraints of 5 kcal/mol/Å<sup>2</sup>, which facilitated the equilibration of solvent molecules around the protein. The resultant system was used for the production simulations at 300 K. For simulation at 360 K, the system was gradually heated from 300 to 360 K over 20 ps with harmonic restraints on the protein, followed by 100 ps equilibration at 360 K in the NPT ensemble. Similarly for the 500 K simulations, the system, which was equilibrated at 360 K, was taken and subjected to gradual heating from 360 to 500 K, followed by a 100 ps equilibration. Production simulations were performed in the NPT ensemble at three different tem-

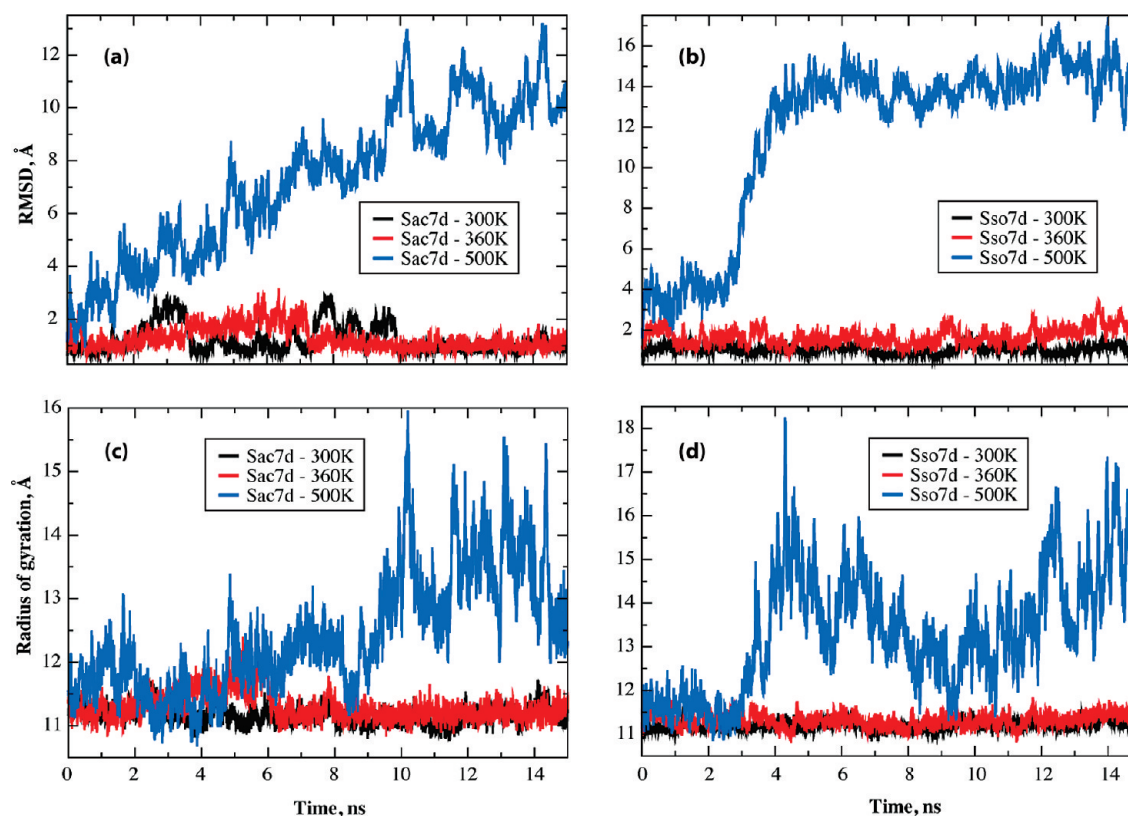


**Figure 2.** Root mean square deviations of the C<sup>α</sup> atoms of Sac7d (a) and Sso7d (b) with respect to the crystal structures and the radius of gyration of Sac7d (c) and Sso7d (d) as a function of time. Black, red, and blue lines represent the data obtained from MD simulations at 300, 360, and 500 K respectively.

peratures (300, 360, and 500 K) starting from an appropriate initial configuration that was obtained from the equilibrium MD simulations at the corresponding temperatures. Temperatures of 300 and 360 K, at which Sac7d and Sso7d were shown to be stable, were chosen to study their differential structural and dynamic behaviors. A temperature of 500 K was used to examine the unfolding of these proteins. The choice of this temperature was based on previous studies which showed that denaturation of proteins may be observed at the nanosecond time scale at 500 K. It should be noted that parametrization of the force field was based on target data from high level quantum mechanical calculations and experiments. Even though the accuracy of force field parameters is not well-known at high temperatures such as 500 K used in this study, previous studies have shown that they can be effectively used for the kind of molecules under study.<sup>35–40</sup> The particle mesh Ewald summation method<sup>54</sup> was employed for the calculation of the electrostatics. In the MD simulations, the Lennard-Jones (LJ) interactions and the real space electrostatic interactions were truncated at 12 Å. For the LJ interactions, a force switch smoothing function from 8 to 10 Å was used, and the nonbond interaction lists were updated heuristically. The simulations used the SHAKE algorithm<sup>55</sup> to constrain the covalent bonds involving hydrogen atoms, which allowed the use of 2 fs as the integration time step. No other restraints/constraints on any part of the system were used in the production simulations. A Nose–Hoover thermostat<sup>56</sup> was used to maintain the temperature, and the Langevin piston algorithm<sup>57</sup> was employed to maintain the pressure at 1 atm.

**Analysis of MD Trajectories.** The analysis of the trajectories was done primarily using the CHARMM program, and the visualization of the snapshots was done using the VMD program,<sup>58</sup> from which figures of three-dimensional structures

were made. The STRIDE algorithm<sup>59</sup> built in VMD was used for the assignment of secondary structure elements for the snapshots in the trajectory. The interaction energies reported in the paper were calculated using the INTER command in CHARMM, which includes the contribution from electrostatic and LJ terms in the force field. The solvent accessible surface area calculations were done using a probe radius of 1.4 Å. The salt bridge was defined based on a distance cutoff value of 6 Å between the participating N (LYS and ARG) and O (ASP and GLU) atoms. The distances between the hydrophobic groups were calculated as the minimum of all possible distances between the non-hydrogen atoms of a given residue pair. The inter residue distances termed as contact maps were obtained based on the pairwise distances between the centers of masses of all the residues. Only those distances less than 12 Å are plotted in Figure 3 for the purpose of clarity. The data presented in the figures and tables were obtained from the last 12 ns of the simulations, unless otherwise noted.

## Results and Discussion

**Overall Structures.** The root-mean-square deviations (rmsd) of the C<sup>α</sup> atoms with respect to the experimental structure obtained for the two proteins at 300, 360, and 500 K are presented in Figure 2. The structures from the 300 and 360 K simulations are in good agreement with the experimental structure exhibiting average rms deviation values between 1.0 and 1.7 Å for both the proteins (Table 1). Experiments, based on differential scanning calorimetry and circular dichroism, have shown that the melting temperatures of Sac7d and Sso7d are 364 and 372 K, respectively.<sup>43–45,60</sup> During the 15 ns MD simulations, the structures of these two proteins are quite stable at 360 K, slightly below their melting temperatures, validating the present results. Low rmsd values at 360 K indicate that the

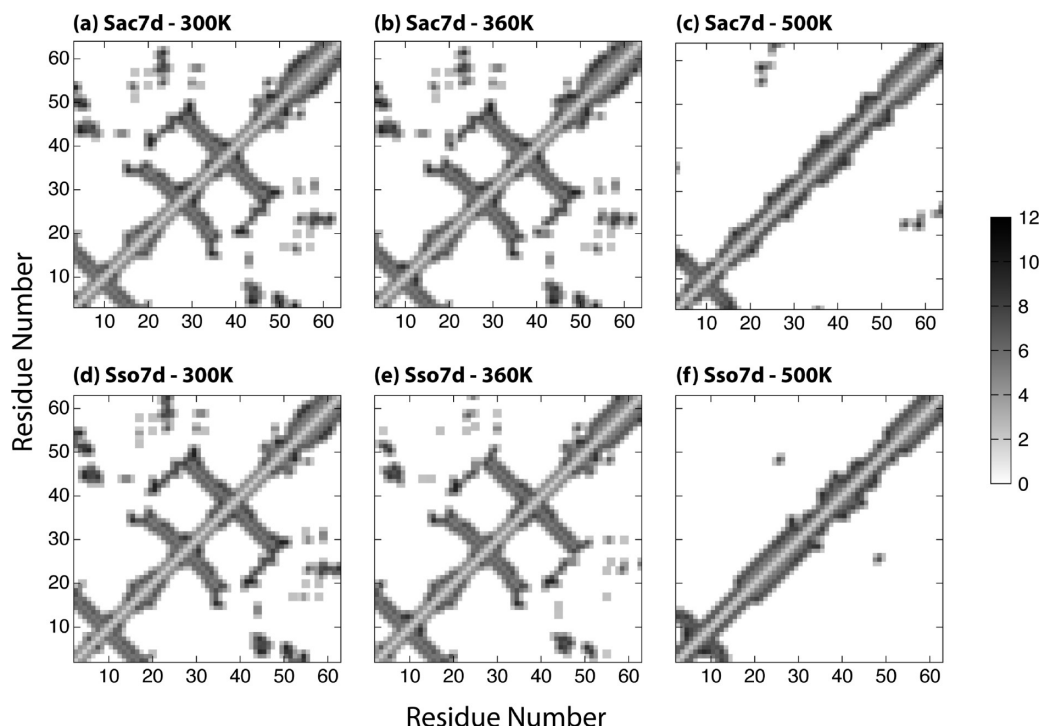


**Figure 3.** Contact maps obtained based on the calculation of the average of the distances between the center of masses of each residue and the other residues obtained during the last 3 ns of the MD simulations. The pairwise distance plots of the Sac7d protein are given in (a), (b), and (c) for the three temperatures 300, 360, and 500 K respectively. Similarly, the plots corresponding to the Sso7d protein are given in (d), (e), and (f).

**TABLE 1: rmsd of the C<sup>α</sup> Atoms with Respect to the Experimental Structure, rmsf of the C<sup>α</sup> Atoms of the Average Structure, Number of Residues Present in β-Sheets, and Number of Residues Present in the α-Helix<sup>a</sup>**

	Sac7d			Sso7d		
	300 K	360 K	500 K	300 K	360 K	500 K
rmsd, Å	1.2 ± 0.1	1.3 ± 0.2	8.2 ± 1.1	1.0 ± 0.0	1.7 ± 0.2	13.8 ± 0.5
radius of gyration, Å	11.1 ± 0.0	11.3 ± 0.1	12.6 ± 0.4	11.2 ± 0.0	11.3 ± 0.0	13.8 ± 0.4
rmsf, Å	1.2	1.4	6.3	1.1	1.4	9.4
# of residues in β-sheets	34.22 ± 0.07	32.67 ± 0.13	15.66 ± 0.9	31.37 ± 0.06	31.31 ± 0.07	7.63 ± 0.81
# of residues in α-helix	11.87 ± 0.03	11.69 ± 0.06	7.69 ± 0.17	9.89 ± 0.02	9.90 ± 0.02	8.27 ± 0.17

<sup>a</sup> The results given are from the last 12 ns of the simulations; the errors represent the standard errors of the mean calculated from every 3 ns blocks.

proteins do not undergo major structural transitions in the time scale of the simulation. In contrast, the rmsd values (Table 1) are quite high at 500 K indicating major structural changes with respect to the experimental structure. The rmsd of Sac7d increases gradually during the 15 ns simulation reaching a maximum of 12.5 Å at about 14 ns (Figure 2a and b). In the simulation involving Sso7d, considerable structural deviation occurs during 2–5 ns (~14 Å) and exhibits a maximum deviation of 17 Å at 14 ns. The calculated radius of gyration values exhibit similar trends, with the 500 K simulations exhibiting larger values (Figure 2c and 2d). While the protein structures are compact at 300 and 360 K similar to the experimental structure, the structures from the 500 K simulations lose their compactness. Overall, the rmsd and radius of gyration analyses indicate that the structures are in the folded state and are closer to the experimental structures at 300 and 360 K. However, at 500 K both the proteins undergo significant structural changes leading to unfolded states (see below).

Contact maps derived from the averages of the inter-residue distances over time illustrate important tertiary contacts present in proteins in general. Figure 3 gives the contact maps of Sac7d and Sso7d at the three different temperatures. Since the proteins undergo major structural changes at 500 K evidenced from rmsd

calculations, the calculations were based only on the trajectories obtained from the last 3 ns of the simulations. The proximity of residues in β1 and β2, β3 and β4, and β4 and β5 found in the experimental structure is quite similar at both 300 and 360 K. The plots also reveal the vicinity of β3 and β5 strands that interact with each other indirectly through β4. Additionally, other tertiary contacts β1–β5, β1-α, and β3-α are well characterized at 300 and 360 K consistent with experimental data. A quick look at Figures 3c and 3f reveals that the three-dimensional structures are drastically different from the starting structure, indicating denaturation. As the protein undergoes unfolding, most of the interactions listed above are destabilized, and the inter-residue distances increase to more than 12 Å. Notably, the β-sheets formed by β1 and β2 strands are quite stable even at 500 K within the length of the simulation performed in this study. Interestingly, residues 20–35 of Sso7d are located close to each other, an observation not found in the structures obtained from experiments or from simulations at 300/360 K. Visualization of the snapshots from the trajectories showed the formation of an α-helix like structure, which is observed in both the proteins (see below).

**Dynamic Features of the Proteins.** The dynamics of the proteins at different temperatures were evaluated based on the

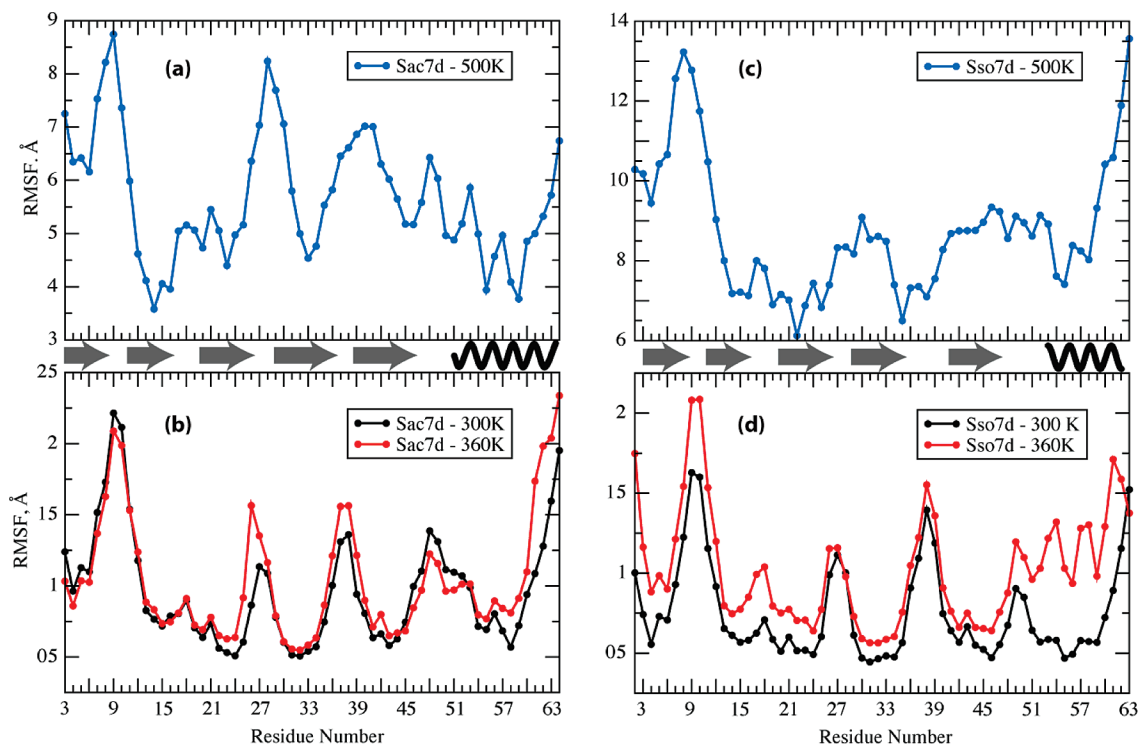


**Figure 4.** Root mean square fluctuations (rmsf) averaged over the residues of Sac7d (a and b), and Sso7d (c and d) proteins. The data obtained from the simulations run at 300, 360, and 500 K are given in black, red, and blue, respectively. Residues as part of the  $\beta$ -sheets and  $\alpha$ -helix in the experimental structure are depicted using arrows and wavy lines, respectively.

root-mean-square fluctuations (rmsf) of the residues (Figure 4). The overall fluctuations obtained at 300 K are similar in Sac7d and Sso7d, and the values increase marginally at 360 K (Table 1). However, the average rmsf values calculated at 500 K are significantly large emphasizing the sampling of larger conformational space at this temperature. The flexibility patterns of the residues of Sac7d and Sso7d are qualitatively similar in both 300 and 360 K simulations (Figure 4b and 4d). The loop and terminal regions are more flexible compared to the rest of the protein, which is expected, since they do not have a large network of tertiary interactions. A notable difference is the high mobility of the  $\alpha$ -helix of Sso7d at 360 K, a feature that is not observed in the 360 K simulation of Sac7d. Also, the flexibility patterns of the  $\alpha$ -helix of Sso7d obtained at 300 and 360 K are slightly different. Sso7d has been shown to exhibit ribonuclease activity,<sup>61</sup> the mechanism of which is not completely understood yet. Previous studies have shown that enzymatic activity of hyperthermophiles is reduced at lower temperatures, and the inherent flexibility, which is reduced at low temperatures, has been suggested as crucial for their functions.<sup>62–65</sup> The difference in the flexibility profiles of Sso7d at 300 and 360 K, observed here, may be related to this phenomenon. Interestingly, the loop region connecting  $\beta_1$  and  $\beta_2$  strands and the residues present before and after the loop region connecting the  $\beta_5$  strand and the  $\alpha$ -helix are more flexible at 300 K compared to those at 360 K. The trends of the rmsf values of the residues calculated at 500 K are quite different from the lower temperatures in addition to the observed higher magnitude (Figure 4a and 4c). However, it should be noted that the rmsf values obtained for the structures from 500 K simulations may not be accurate since the alignment was done on structurally diverse conformations/unfolded states.

**Hierarchical Unfolding Pathway.** The nature of the structural transitions via unfolding during the simulations was investigated by examining the evolution of the secondary

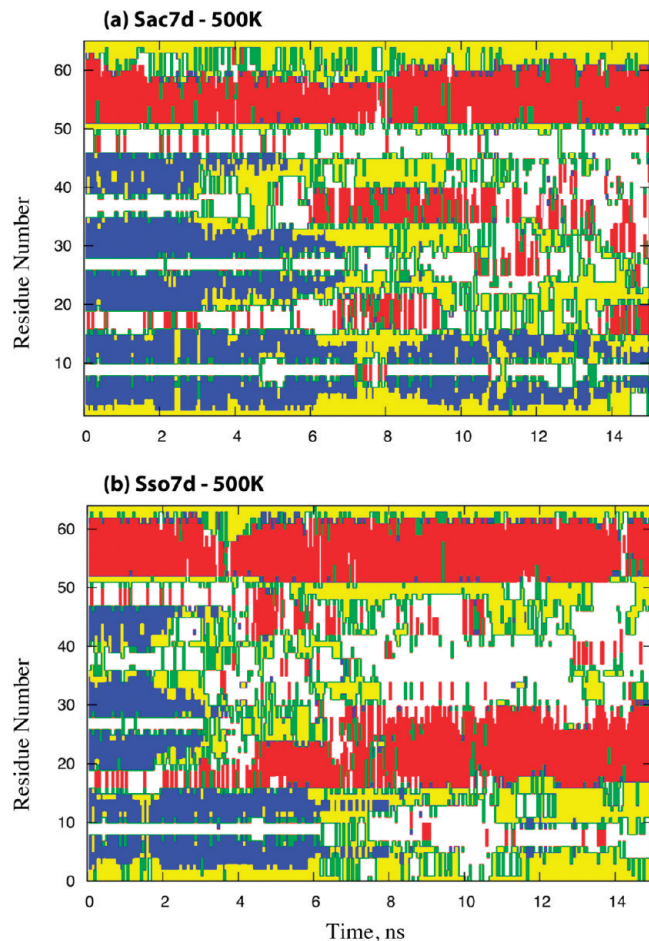


**Figure 5.** Evolution of the secondary structure of Sac7d (a) and Sso7d (b) with respect to time obtained at 500 K.  $\beta$ -sheets,  $\alpha$ -helices, coils, turns, and 3–10 helices are given in blue, red, yellow, white, and green, respectively.

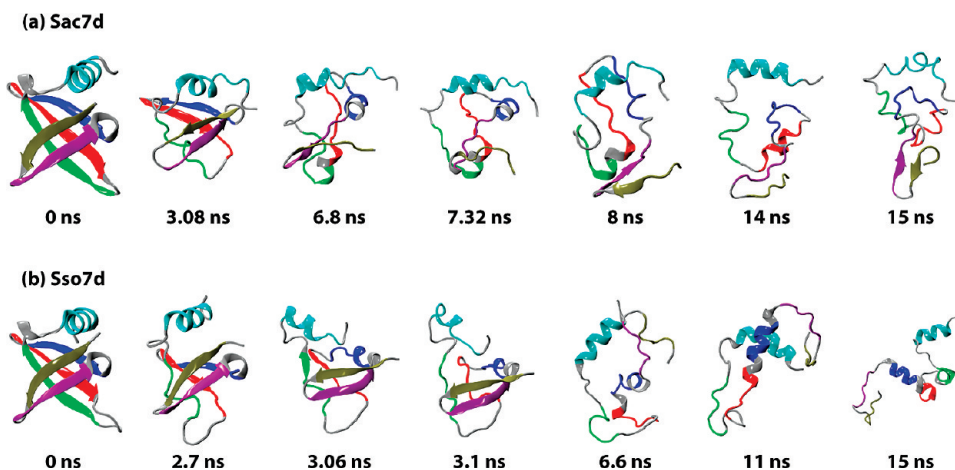


**Figure 6.** Select snapshots of the three-dimensional structures of Sac7d (a) and Sso7d (b) illustrating the unfolding pathway.  $\beta_1$ ,  $\beta_2$ ,  $\beta_3$ ,  $\beta_4$ ,  $\beta_5$ , and  $\alpha$  in the starting structure are represented by yellowish green, purple, blue, red, green, and cyan colors, respectively.

**TABLE 2: Average Interaction Energies (kcal/mol) of the Main Secondary Structure Elements with Respect to Each Other Calculated from the Last 12 ns of the Simulations**

	Sac7d			Sso7d		
	300 K	360 K	500 K	300 K	360 K	500 K
$\beta_1-\beta_2$	$-483.9 \pm 12.1$	$-527.7 \pm 8.0$	$-516.6 \pm 12.6$	$-327.8 \pm 5.7$	$-348.8 \pm 3.5$	$-281.5 \pm 29.6$
$\beta_1-\beta_3$	$120.1 \pm 1.3$	$124.2 \pm 0.4$	$130.5 \pm 5.4$	$79.4 \pm 0.6$	$78.4 \pm 0.5$	$81.7 \pm 1.2$
$\beta_1-\beta_4$	$-115.6 \pm 1.8$	$-121.2 \pm 0.8$	$-247.3 \pm 50.1$	$-74.0 \pm 1.2$	$-74.5 \pm 0.4$	$-45.8 \pm 5.8$
$\beta_1-\beta_5$	$85.0 \pm 2.6$	$84.1 \pm 1.8$	$178.6 \pm 26.2$	$54.5 \pm 2.0$	$53.1 \pm 1.0$	$40.4 \pm 3.4$
$\beta_1-\alpha_1$	$-4.1 \pm 4.1$	$-7.5 \pm 4.1$	$-2.8 \pm 4.2$	$0.5 \pm 1.9$	$2.3 \pm 1.2$	$-9.8 \pm 4.9$
$\beta_2-\beta_3$	$-128.2 \pm 0.4$	$-128.2 \pm 1.1$	$-156.9 \pm 9.3$	$-124.7 \pm 0.8$	$-126.3 \pm 1.6$	$-219.3 \pm 25.3$
$\beta_2-\beta_4$	$103.6 \pm 1.5$	$94.9 \pm 10.1$	$208.5 \pm 30.3$	$82.1 \pm 5.9$	$83.4 \pm 6.7$	$87.9 \pm 12.4$
$\beta_2-\beta_5$	$-89.9 \pm 1.3$	$-86.4 \pm 2.0$	$-235.7 \pm 28.5$	$-87.8 \pm 1.9$	$-86.7 \pm 1.1$	$-75.5 \pm 8.7$
$\beta_2-\alpha_1$	$11.6 \pm 6.2$	$11.6 \pm 4.1$	$-0.2 \pm 4.9$	$1.6 \pm 2.8$	$1.2 \pm 0.9$	$-53.0 \pm 12.8$
$\beta_3-\beta_4$	$-229.4 \pm 7.7$	$-228.4 \pm 3.8$	$-167.4 \pm 34.4$	$-217.2 \pm 2.5$	$-216.3 \pm 1.4$	$-196.6 \pm 35.5$
$\beta_3-\beta_5$	$116.0 \pm 2.0$	$116.9 \pm 3.8$	$96.3 \pm 5.6$	$110.2 \pm 3.0$	$107.3 \pm 1.9$	$109.4 \pm 12.4$
$\beta_3-\alpha_1$	$-43.0 \pm 1.1$	$-48.3 \pm 9.2$	$-91.6 \pm 22.4$	$-47.1 \pm 5.4$	$-77.8 \pm 4.2$	$-67.0 \pm 17.6$
$\beta_4-\beta_5$	$-229.1 \pm 11.0$	$-206.7 \pm 9.0$	$-198.9 \pm 20.3$	$-213.1 \pm 9.6$	$-209.9 \pm 8.1$	$-216.2 \pm 35.4$
$\beta_4-\alpha_1$	$-1.3 \pm 1.8$	$1.2 \pm 1.3$	$-8.3 \pm 7.0$	$-3.7 \pm 0.9$	$-1.5 \pm 0.7$	$-2.0 \pm 2.8$
$\beta_5-\alpha_1$	$-7.8 \pm 1.2$	$-8.0 \pm 1.0$	$1.5 \pm 2.4$	$-4.8 \pm 0.6$	$-4.4 \pm 0.5$	$-0.5 \pm 2.3$

structure as a function of time. The secondary structure is quite conserved over time at both 300 and 360 K (Figures S1 and S2 in Supporting Information). The average number of residues that are conserved in  $\beta$ -sheets and the  $\alpha$ -helix is given in Table 1 for comparison between the different simulations. The number averages in both the proteins at 300 and 360 K are similar, confirming minor structural differences. On the contrary, both Sac7d and Sso7d lose their original secondary structure elements considerably at 500 K (Figure 5). Remarkably, the orders in which they lose their secondary elements are quite similar to each other. Select three-dimensional structures that signify the unfolding of the two proteins are given in Figure 6. Of all the structural elements in the proteins, the  $\alpha$ -helix seems to be the most stable within the time scale of the simulation retaining its structure to a larger extent especially in Sso7d. The terminal residues of the  $\alpha$ -helix of Sac7d undergo unfolding and keep fluctuating between the native  $\alpha$ -helical form and coil. Such an effect is less pronounced in Sso7d, which is probably due to the differences in the sequences and the lengths of the  $\alpha$ -helix of the two proteins. Initially,  $\beta_5$  undergoes unfolding in both the proteins leading to disorders in the  $\beta$ -sheet formed by  $\beta_3-5$  strands. This is followed by simultaneous unfolding of  $\beta_4$  and  $\beta_5$  resulting in the complete loss of the  $\beta$ -sheet structure consisting of these strands ( $\beta_3-5$ ). In both the proteins, the denaturation of the  $\beta$ -sheet is accompanied by partial unfolding of the  $\alpha$ -helix (Figures 5 and 6). Further analysis indicated that intramolecular interactions are observed to be responsible for

the coupling of the unfolding of the  $\beta$ -sheet formed by  $\beta_3-5$  with the partial unfolding of the  $\alpha$ -helix (see below). Finally, the  $\beta$ -sheet comprising  $\beta_1$  and  $\beta_2$ , which was originally packed against the other  $\beta$ -sheet, unfolds. However, they undergo transitions between the folded and the unfolded form, particularly in Sac7d. During this process, the  $\alpha$ -helix, which was partially unfolded during the denaturation of  $\beta_3-5$ , undergoes structural changes and refolds to its original conformational state. Notably,  $\beta_3$  and  $\beta_4$  along with the connecting loop tend to fold to an  $\alpha$ -helical form after they have unfolded (Figures 5 and 6). The thermal-induced unfolding of these two homologous proteins reveals striking resemblances between the two pathways. Such an atomic level similarity between these two hierarchical unfolding pathways is also explained well by the temperature-dependent intermolecular interactions, which is discussed in the following section.

**Intramolecular Interactions.** Intermolecular interactions between various secondary structural elements constituted in a protein are crucial for its overall stability. The interaction energies between the major secondary elements ( $\beta_1-5$  and  $\alpha$ ) were calculated to identify the principal interactions responsible for the thermal stability, to understand the unfolding pathways of Sac7d and Sso7d, and to identify the energetic determinants responsible for such a hierarchical unfolding (Table 2). Most of the intramolecular interaction energies are less favorable in Sso7d compared to Sac7d at 300 and 360 K. Given the conservation of structures of these two proteins, it is tempting

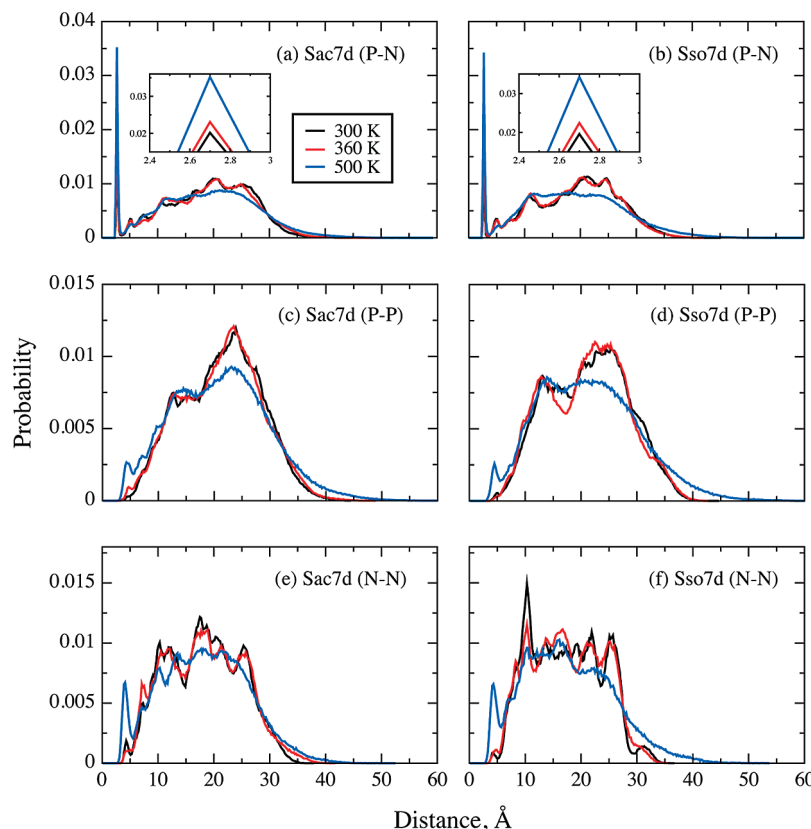


**Figure 7.** Probability distributions corresponding to the interatomic distances of positive–negative, P–N (a, b), positive–positive, P–P (c, d), and negative–negative, N–N (e, f) residue pairs of Sac7d (a, c, e) and Sso7d (b, d, f) proteins.

to conclude that Sac7d is more stable than Sso7d based on these interaction energies. However, the observed melting temperature of Sso7d is marginally higher than that of Sac7d.<sup>43–45,60</sup> In contrast, an experimental study based on circular dichroism spectroscopy and differential scanning calorimetry suggested that even though the melting temperature of Sso7d is high the intrinsic stability of the protein is low.<sup>60</sup> They also showed that Sso7d is poorly stabilized at the maximum physiological growth temperature of *Sulfolobus solfataricus*. The low favorable interaction energies in Sso7d compared to Sac7d may also be responsible for the faster unfolding of the former during the MD simulations (Figures 5 and 6). However, additional MD simulations are needed to confirm this effect. Overall, favorable intramolecular interactions (sum of the energy values along the columns in Table 2) increase from 300 to 360 K indicating that the proteins are stabilized at 360 K, close to the organisms’ physiological growth temperature.

The favorable interaction energies of  $\beta$ 5 with  $\beta$ 4 and  $\beta$ 2 reduce marginally at 360 K compared to at 300 K. All the other favorable interaction energies are almost the same at these two temperatures or become more favorable at 360 K leading to higher stability. The decrease in the interaction of  $\beta$ 5 with the other parts of the protein with increase in the temperature explains the observation that this is the first to undergo unfolding. The  $\alpha$ -helix has significant stabilizing interactions, and only with  $\beta$ 3 it becomes more favorable at 360 K with respect to at room temperature. These strong interactions are proposed as reasons behind the coupling of the unfolding of  $\beta$ 3–4 and the partial unfolding of the  $\alpha$ -helix. Overall, increase in the favorable interaction energies at 360 K with respect to 300 K is suggested to be responsible for the high stability of these two proteins. The interaction energies obtained at 500 K are more stabilizing in general. It should be noted that the

energies correspond to three-dimensional structures of the proteins that have changed significantly due to unfolding at 500 K.

**Salt Bridge Networks.** Salt bridge networks, which were shown to be more prevalent in thermophilic and hyperthermophilic proteins compared to their mesophilic counterparts, were identified as one of the primary factors responsible for their high thermal stability.<sup>15,16,27–29</sup> However, few reports have suggested that they have a destabilizing effect due to the enormous desolvation penalty involved in the formation of salt bridges. The structural parameters and energetic contributions of the salt bridges to the stabilization of the two proteins are discussed here. The probability distributions of all possible N(LYS/ARG)-O(ASP/GLU) interatomic distances were computed and given in Figure 7a and b. Sharp peaks at about 2.7 Å correspond to the most stable salt bridge formed between a positive–negative residue pair. The magnitudes of the peaks display interesting trends (see insets in the figure)—with an increase in the temperature, the magnitude increases illustrating the strengthening of the noncovalent interactions. A closer look at the time vs distance plots (Figure S3–8 in Supporting Information) shows that the increase in the probability at 500 K is primarily due to the new salt bridges that are formed during denaturation. However, the salt bridge networks are similar at 300 and 360 K, and tightening of the interactions is indeed observed at 360 K. The effect of any unfavorable electrostatic interactions between like-charged residues (positive–positive and negative–negative residue pairs) was investigated via the calculation of probability distributions of distance corresponding to N–N(LYS/ARG) and O–O(ASP-GLU). Similar distribution curves were obtained for these distances at 300 and 360 K (Figure 7c–f) indicating minimal effect of temperature on the repulsive interactions. Explicit calculation of the interaction

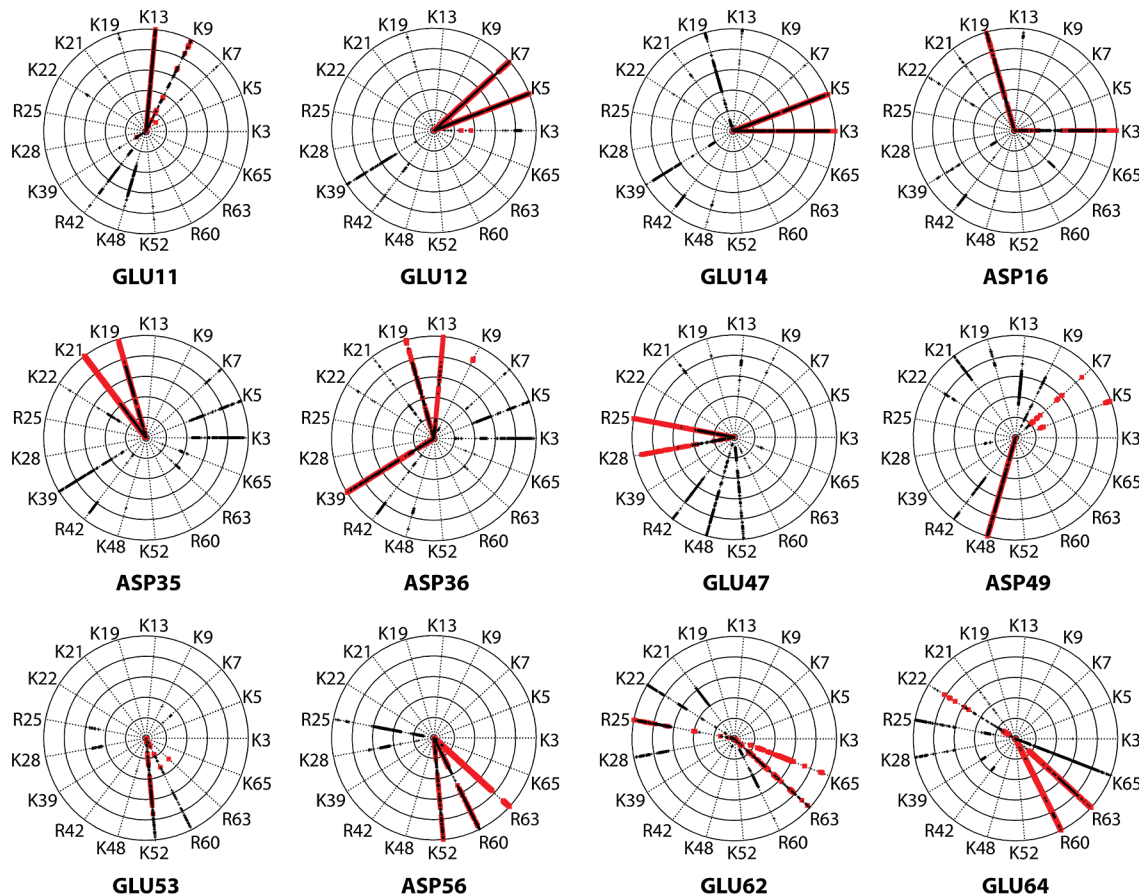


**Figure 8.** Plots showing the salt bridge networks of Sac7d at 300 and 500 K. In each of the circular plots, the center represents  $t = 0$ , and the outermost circle represents  $t = 15$  ns. Each plot gives information on the existence/nonexistence of salt bridge interaction between each of the negative residues and all other positive residues present in the protein. The presence of a data point (red at 300 K and black at 500 K) along the spokes indicates salt bridging interaction (less than 6 Å) between the corresponding positive and negative residue pairs.

energies confirmed these observations. However, a significant increase in the probabilities corresponding to shorter distances was observed at 500 K. Hence, there is a notable increase in both electrostatic attractive and repulsive interactions at 500 K. The change in the nature of salt bridge networks was further analyzed based on the time vs distance plots.

The distances between the positive and negative residues as a function of time are given in Figure S3-8 in the Supporting Information. The plots obtained from 300 and 360 K simulations are similar to each other further confirming identical three-dimensional structures at these two temperatures. Select plots obtained using the simulations at 300 and 500 K are presented in Figures 8 and 9. In the figure, the presence of a data point indicates that the distance between the N of LYS/ARG and O of ASP/GLU is less than 6 Å (see figure legend for more details). Several new salt bridges are formed while unfolding at 500 K. For example, GLU47 of Sac7d exhibits ionic interactions with LYS28 and ARG25 in the experimental structure, which is also sufficiently sampled in the MD simulations at both 300 and 360 K. In contrast, both these salt bridges were disrupted at 500 K and new networks involving LYS9, LYS13, LYS19, LYS21, ARG42, LYS48, LYS52, ARG60, and ARG65. In general, the lifetimes of a given salt bridge, both the ones present in the original folded state and the ones that were formed during denaturation, are short at 500 K. The higher frequency of new salt bridge formation in explicit solvent environment also supports the previous proposal that the desolvation penalty is less at elevated temperatures and has less influence on the actual formation of the network. Hence, the

increase in the probabilities of the salt bridge distances at 500 K (Figure 7e and f) is mainly due to the intermittent formation of new contacts rather than strengthening of the existing ones. However, the increase in the probabilities at 360 K is due to the tightening of the existing salt bridges (Figure S3-8 in Supporting Information).

The energetic contributions of the salt bridges were evaluated by calculating the sum of interaction energies of all positive-negative residue pairs (Table 3). The energies corresponding to the individual pairs of all the residues are tabulated in the Supporting Information (Table S1). The favorable interaction energies between the positive and negative residues increase while going from 300 to 360 K further confirming the stabilizing effect observed above based on histogram plots. These interactions increase substantially at 500 K due to the new salt bridges formed while denaturing. Interestingly, the repulsion energies between the positive-positive residues decrease while going from 300 to 360 K in both the proteins. However, the repulsion interaction energies between the negative residues remain similar at 300 and 360 K. Overall, the calculated geometric and energetic parameters indicate that the salt bridges are more stable at 360 K compared to at 300 K contributing toward the higher stability of the proteins. Additionally, the repulsion interactions between the positively charged residues are marginally reduced at 360 K. Hence, the salt bridges not only help the structure from denaturing at 360 K but also enhance the stability of the proteins compared to their stability at room temperature.

**Hydrophobic Core.** In addition to the salt bridge networks, a highly compact hydrophobic core has been suggested to be

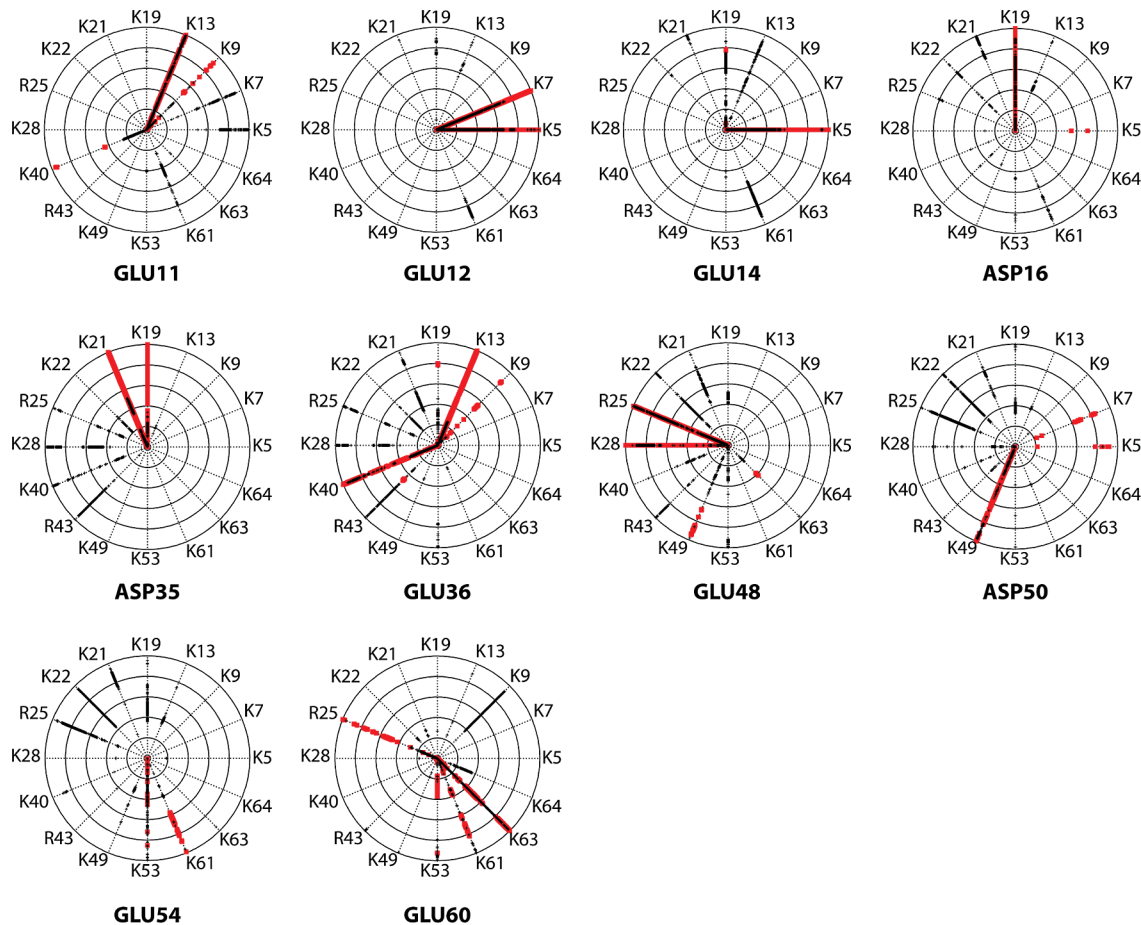


**Figure 9.** Plots showing the salt bridge networks of Sso7d at 300 and 500 K. In each of the circular plots, the center represents  $t = 0$ , and the outermost circle represents  $t = 15$  ns. Each plot gives information on the existence/nonexistence of salt bridge interaction between each of the negative residues and all other positive residues present in the protein. The presence of a data point (red at 300 K and black at 500 K) along the spokes indicates salt bridging interaction (less than 6 Å) between the corresponding positive and negative residue pairs.

**TABLE 3: Average of the Sum of the Interaction Energies (kcal/mol) between Positive–Positive (P–P), Negative–Negative (N–N), Positive–Negative (P–N), and Hydrophobic–Hydrophobic (HP–HP) Residue Pairs<sup>a</sup>**

	Sac7d			Sso7d		
	300 K	360 K	500 K	300 K	360 K	500 K
P–P	$-2043.6 \pm 13.0$	$-2026.7 \pm 26.1$	$-2160.0 \pm 48.7$	$-1715.2 \pm 25.5$	$-1685.1 \pm 11.9$	$-1799.9 \pm 16.2$
N–N	$1235.7 \pm 1.2$	$1238.8 \pm 4.8$	$1355.0 \pm 51.7$	$870.8 \pm 6.1$	$870.4 \pm 6.3$	$925.7 \pm 15.6$
P–N	$-4405.9 \pm 27.8$	$-4457.7 \pm 36.5$	$-5037.0 \pm 137.8$	$-3392.9 \pm 35.1$	$-3460.6 \pm 26.2$	$-3903.9 \pm 62.1$
HP–HP	$-92.2 \pm 0.3$	$-88.4 \pm 0.4$	$-56.5 \pm 4.4$	$-90.1 \pm 0.6$	$-84.9 \pm 0.9$	$-50.1 \pm 1.6$

<sup>a</sup> The results given are from the last 12 ns of the simulations; the errors represent the standard errors of the mean calculated from every 3 ns blocks.

one of the factors responsible for enhanced thermal stability of thermophilic proteins. In Sac7d and Sso7d, such a hydrophobic core exists in the interface of the  $\beta$ -sheets and the  $\alpha$ -helix (Figure 10a). The shortest distance between the non-hydrogen atoms in each of the hydrophobic residue pairs was computed, and the corresponding probability distributions are given in Figure 10b and 10c. All the distances were found to be less than 15 Å in the 300 and 360 K simulations with the maximum probabilities occurring at about 2.5 Å. This indicates strong interactions among the residues forming the core of the proteins. These distances extend to up to 35 Å at 500 K indicating a decrease in the contribution of the stability of the proteins due to the hydrophobic core. The sums of the average interaction energies between all possible pairs were calculated (Table 3). The favorable interaction energies due to the hydrophobic core marginally decrease from 300 to 360 K associated with a slight decrease in the probability corresponding to 2.5 Å at 360 K.

However, these interactions are significantly reduced at 500 K. Notably, the magnitudes of the stabilization energies due to the hydrophobic core are much less compared to those due to the salt bridge networks. However, the contribution from the solvation of charged residues is clearly different from that of the hydrophobic residues, and these effects are discussed below.

**Solvation Properties.** Solvent accessible surface area (SASA) calculations were performed to understand the solvation properties of these proteins at different temperatures (Table 4). SASA calculations of the whole proteins are comparable to each other at 300 and 360 K, and expectedly the values are considerably higher at 500 K. SASA values have also been calculated for the individual secondary structure elements. Notable is the increase in the surface area corresponding to  $\beta$ 5 in both the proteins at 360 K with respect to that at 300 K. The exposure of  $\beta$ 5 is traced to its reduced interaction with  $\beta$ 4, at 360 K. This further supports the observation that the unfolding of the

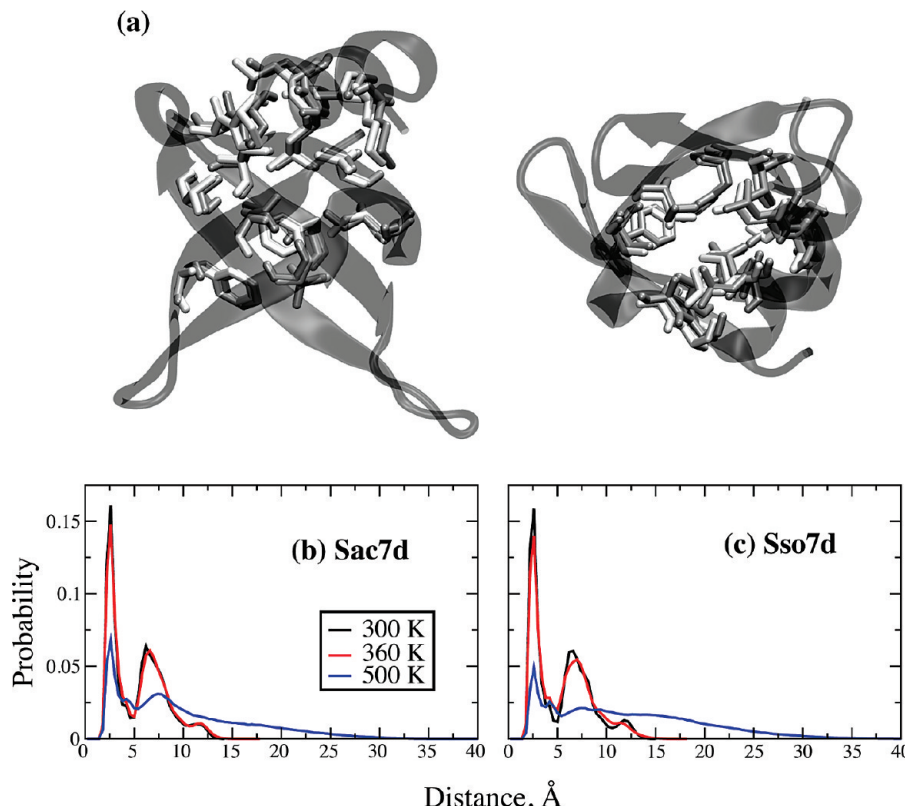


**Figure 10.** (a) Hydrophobic residues that form the core of Sac7d (gray) and Sso7d (white) given in stick representations and the superposition of their three structures. Cartoon structure of only Sso7d is shown for clarity. Probability distributions of the minimum distances between each hydrophobic–hydrophobic residue pair of Sac7d (b) and Sso7d (c). Data from 300, 360, and 500 K simulations are given in black, red, and blue colors, respectively.

**TABLE 4: Average Solvent Accessible Surface Areas ( $\text{\AA}^3$ ) Calculated for the Protein, Various Secondary Structure Regions, and Positive (P), Negative (N), and Hydrophobic (HP) Residues<sup>a</sup>**

	Sac7d			Sso7d		
	300 K	360 K	500 K	300 K	360 K	500 K
protein	4986 ± 18	5047 ± 27	5703 ± 164	5031 ± 22	4868 ± 26	5876 ± 164
$\beta 1$	471 ± 3	490 ± 12	681 ± 24	377 ± 5	372 ± 3	578 ± 31
$\beta 2$	431 ± 3	421 ± 7	354 ± 36	496 ± 6	486 ± 1	514 ± 12
$\beta 3$	571 ± 3	604 ± 9	633 ± 45	553 ± 5	541 ± 5	618 ± 45
$\beta 4$	224 ± 4	238 ± 6	575 ± 73	349 ± 8	349 ± 3	809 ± 42
$\beta 5$	441 ± 11	485 ± 7	564 ± 21	574 ± 8	593 ± 5	629 ± 26
$\alpha$	1024 ± 21	994 ± 5	1149 ± 33	872 ± 7	884 ± 13	1033 ± 64
P	2552 ± 9	2508 ± 7	2197 ± 63	2406 ± 7	2242 ± 14	1980 ± 87
N	1017 ± 9	1008 ± 9	925 ± 63	895 ± 14	845 ± 8	717 ± 22
HP	225 ± 2	221 ± 10	977 ± 155	209 ± 5	207 ± 5	1234 ± 68

<sup>a</sup> The results given are from the last 12 ns of the simulations; the errors represent the standard errors of the mean calculated from every 3 ns blocks.

proteins initiates from  $\beta 5$ . The SASA values of the charged residues decrease at 360 K compared to 300 K. The charged residues, which are less exposed to the solvent environment in turn, are capable of stronger salt bridge interactions as shown before. Interestingly, at 500 K where the overall protein is highly exposed to the solvent in its unfolded state, the SASA values of charged residues are lower compared to at 300/360 K. This phenomenon is related to the previous discussion that at high temperatures the desolvation penalty of charged residues decreases facilitating the formation of salt bridges. Thus, solvation properties reveal the importance of hydrophobic interactions in the stabilization of these proteins at nonphysiological temperatures. SASA values of the residues that form the hydrophobic core are similar (marginally less) in both the proteins at 360 K with respect to that at 300 K. In contrast, the surface areas computed at 500 K are about 5–6 larger. The

larger accessible nature of these hydrophobic residues in the unfolded form greatly contributes toward high instability due to unfavorable interactions with water. Hence, the maintenance of these residues as a core in the interior of the proteins is crucial for their stability. The salt bridges on the surface which gets more stabilized at 360 K are proposed to be highly responsible for keeping this in tact.

## Conclusions

Hyperthermophilic chromosomal proteins Sac7d and Sso7d were studied using MD simulations performed at three different temperatures. Consistent with experimental observations, these proteins are significantly stable at high temperature (360 K) and denature at extreme temperature (500 K). The deviations of the three-dimensional structures obtained using the MD simulations

are low and comparable at 300 and 360 K for both proteins with respect to the experimental structures. The differential dynamic patterns of Sso7d are proposed to be related to the ribonuclease activity of this protein. Contact maps and the evolution of secondary structural elements as a function of the simulation time at 500 K reveal hierarchical unfolding pathways common to the two proteins.  $\beta$ 5 unfolds first followed by  $\beta$ 3 and  $\beta$ 4 associated by the partial unfolding of the  $\alpha$ -helix, and finally  $\beta$ 1 and  $\beta$ 2 undergo denaturation associated by the refolding of the  $\alpha$ -helix to its native form. Similar hierarchical unfolding events, and rather high stability of the  $\beta$ -sheet formed by  $\beta$ 1 and  $\beta$ 2 strands, is supported by the differential interaction energies and the effect of the increase in temperature. It will be interesting to see if any future experimental study would support the thermally induced unfolding mechanism hypothesized here. Geometric analysis of the salt bridges indicates their strengthening at 360 K and lower lifetime at 500 K. During the course of unfolding at 500 K, several new and nonspecific salt bridges are formed that are associated with significant changes in the three-dimensional structures. Comparison of the interaction energies between charged residues at different temperatures reveals strengthening of the salt bridges and lowering of repulsive interactions between like-charged residues at 360 K, closer to the organism's physiological growth temperature. Hence, the salt bridges seem crucial in maintaining the three-dimensional structures in their native states at elevated temperatures. As noted above, minor changes in the structures and other properties are observed from 300 and 360 K simulations. However, the subtle effects of tightening of the salt bridges at 360 K and the differences in the intramolecular energies explaining unfolding pathways are seen in both the proteins suggesting that the issue of sampling may not alter the conclusions obtained here. Stability of the compact hydrophobic core of the proteins and its effect on the overall stabilization are not affected when going from 300 to 360 K, and the magnitudes of these interactions are smaller compared to salt bridges. However, the solvent accessible surface area values indicate that the maintenance of the hydrophobic core is essential to avoid unfavorable interactions between these residues and the solvent. A significant decrease in the SASA of the charged residues at high temperature supports previous studies that the solvation penalty is lower, and hence the formation of salt bridges is more favorable. Additionally, 500 K simulations indicate intermittent and frequent formation of new salt bridges during the unfolding process and support this phenomenon.

**Acknowledgment.** We thank DAE-BRNS, DST, and IIIT-H for financial assistance.

**Supporting Information Available:** Figures of the evolution of secondary structure elements of Sac7d and Sso7d with respect to time, distance plots corresponding to salt bridges, and tables of inter-residue interaction energies. This material is available free of charge via the Internet at <http://pubs.acs.org>.

## References and Notes

- (1) Rothschild, L.; Mancinelli, R. *Nature* **2001**, *409*, 1092.
- (2) Horikoshi, K.; Grant, W. *Extremophiles: microbial life in extreme environments*; Wiley-Liss, 1998.
- (3) Vieille, C.; Zeikus, G. *Microbiol. Mol. Biol. Rev.* **2001**, *65*, 1.
- (4) Sternen, R.; Liebl, W. *Crit. Rev. Biochem. Mol. Biol.* **2001**, *36*, 39.
- (5) Unsworth, L.; van der Oost, J.; Koutsopoulos, S. *FEBS J.* **2007**, *274*, 4044.
- (6) Luke, K.; Higgins, C.; Wittung-Stafshede, P. *FEBS J.* **2007**, *274*, 4023.
- (7) Zierenberg, R. A.; Adams, M. W. W.; Arp, A. J. *Proc. Natl. Acad. Sci. U.S.A.* **2000**, *97*, 12961.
- (8) Robinson, H.; Gao, Y.; McCrary, B.; Edmondson, S.; Shriner, J.; Wang, A. *Nature* **1998**, *392*, 202.
- (9) Mukherjee, A.; Sokunbi, A. O.; Grove, A. *Nucleic Acids Res.* **2008**, *36*, 3956.
- (10) Ishikawa, K.; Okumura, M.; Katayanagi, K.; Kimura, S.; Kanaya, S.; Nakamura, H.; Morikawa, K. *J. Mol. Biol.* **1993**, *230*, 529.
- (11) Katayanagi, K.; Miyagawa, M.; Matsushima, M.; Ishikawa, M.; Kanaya, S.; Nakamura, H.; Ikebara, M.; Matsuzaki, T.; Morikawa, K. *J. Mol. Biol.* **1992**, *223*, 1029.
- (12) Demirjian, D.; Mor s-Varas, F.; Cassidy, C. *Curr. Opin. Chem. Biol.* **2001**, *5*, 144.
- (13) Haki, G.; Rakshit, S. *Bioresour. Technol.* **2003**, *89*, 17.
- (14) Niehaus, F.; Bertoldo, C.; Kähler, M.; Antranikian, G. *Appl. Microbiol. Biotechnol.* **1999**, *51*, 711.
- (15) Chakravarty, S.; Varadarajan, R. *Biochemistry* **2002**, *41*, 8152.
- (16) Gianese, G.; Bossa, F.; Pascarella, S. *Proteins: Struct., Func., Genet.* **2002**, *47*, 236.
- (17) Haney, P.; Stees, M.; Konisky, J. *J. Biol. Chem.* **1999**, *274*, 28453.
- (18) Szilágyi, A.; Závodszky, P. *Structure* **2000**, *8*, 493.
- (19) Vogt, G.; Woell, S.; Argos, P. *J. Mol. Biol.* **1997**, *269*, 631.
- (20) Suhré, K.; Claverie, J. *J. Biol. Chem.* **2003**, *278*, 17198.
- (21) Karshikoff, A.; Ladenstein, R. *Trends Biochem. Sci.* **2001**, *26*, 550.
- (22) Gianese, G.; Argos, P.; Pascarella, S. *Protein Eng.* **2001**, *14*, 141.
- (23) Kannan, N.; Vishveshwara, S. *Protein Eng.* **2000**, *13*, 753.
- (24) Kumar, S.; Tsai, C.-J.; Nussinov, R. *Protein Eng.* **2000**, *13*, 179.
- (25) Dominy, B. N.; Minoux, H.; III, C. L. B. *Proteins: Struct., Funct., Bioinf.* **2004**, *57*, 128.
- (26) Thomas, A. S.; Elcock, A. H. *J. Am. Chem. Soc.* **2004**, *126*, 2208.
- (27) Missimer, J.; Steinmetz, M.; Baron, R.; Winkler, F.; Kammerer, R.; Daura, X.; van Gunsteren, W. *Protein Sci.: Publ. Protein Soc.* **2007**, *16*, 1349.
- (28) Ge, M.; Xia, X.; Pan, X. *J. Biol. Chem.* **2008**, *283*, 31690.
- (29) Folch, B.; Rooman, M.; Dehouck, Y. *J. Chem. Inf. Model.* **2007**, *48*, 119.
- (30) Gromiha, M. *Biophys. Chem.* **2001**, *91*, 71.
- (31) Querol, E.; Perez-Pons, J.; Mozo-Villarias, A. *Protein Eng. Des. Sel.* **1996**, *9*, 265.
- (32) Spassov, V. Z.; Karshikoff, A. D.; Ladenstein, R. *Protein Sci.* **1995**, *4*, 1516.
- (33) *Computational biochemistry and biophysics*; Becker, O. M., Mackrell, A. D., Roux, B., Watanabe, M., Eds.; CRC: New York, 2001.
- (34) *Handbook of molecular biophysics: Methods and applications*; Bohr, H. G., Ed.; Wiley: New York, 2009.
- (35) de Bakker, P.; Hunenberger, P.; McCammon, J. *J. Mol. Biol.* **1999**, *285*, 1811.
- (36) Merlini, A.; Graziano, G.; Mazzarella, L. *Proteins: Struct., Funct., Bioinf.* **2004**, *57*, 692.
- (37) Liu, J.; Yu, H.; Shen, Z. *J. Mol. Graphics Modell.* **2008**, *27*, 529.
- (38) Tang, L.; Liu, H. *Journal Biomol. Struct. Dyn.* **2007**, *24*, 379.
- (39) Lazaridis, T.; Lee, I.; Karplus, M. *Protein Sci.* **1997**, *6*, 2589.
- (40) Danciulessu, C.; Ladenstein, R.; Nilsson, L. *Biochemistry* **2007**, *46*, 8537.
- (41) Caflisch, A.; Karplus, M. *Proc. Natl. Acad. Sci.* **1994**, *91*, 1746.
- (42) Tirado-Rives, J.; Orozco, M.; Jorgensen, W. *Biochemistry* **1997**, *36*, 7313.
- (43) Clark, A. T.; McCrary, B. S.; Edmondson, S. P.; Shriner, J. W. *Biochemistry* **2004**, *43*, 2840.
- (44) McCrary, B. S.; Edmondson, S. P.; Shriner, J. W. *J. Mol. Biol.* **1996**, *264*, 784.
- (45) Bedell, J.; Edmondson, S.; Shriner, J. *Biochemistry* **2005**, *44*, 915.
- (46) Needleman, S. *J. Mol. Biol.*, **48**, 443.
- (47) Brooks, B. R.; III, C. L. B.; Mackerell, A. D.; Nilsson, L.; Petrella, R. J.; Roux, B.; Won, Y.; Archontis, G.; Bartels, C.; Boresch, S.; Caflisch, A.; Caves, L.; Cui, Q.; Dinner, A. R.; Feig, M.; Fischer, S.; Gao, J.; Hodoscek, M.; Im, W.; Kuczera, K.; Lau, F. T. K.; Mattos, C.; Michnick, S.; Ngo, T.; Nguyen, T. D.; Prudhomme, B.; Reiher, W. E.; Roux, B.; Schlenkrich, M.; Smith, J. C.; Stote, R.; Straub, J.; Watanabe, M.; Wiorkiewicz-Kuczera, J.; Yin, D.; Karplus, M. *J. Phys. Chem. B* **1998**, *102*, 3586.
- (48) MacKerell, A. D.; Bashford, D.; Bellott, Dunbrack, R. L.; Evanseck, J. D.; Field, M. J.; Fischer, S.; Gao, J.; Guo, H.; Ha, S.; Joseph-McCarthy, D.; Kuchnir, L.; Kuczera, K.; Lau, F. T. K.; Mattos, C.; Michnick, S.; Ngo, T.; Nguyen, T. D.; Prudhomme, B.; Reiher, W. E.; Roux, B.; Schlenkrich, M.; Smith, J. C.; Stote, R.; Straub, J.; Watanabe, M.; Wiorkiewicz-Kuczera, J.; Yin, D.; Karplus, M. *J. Phys. Chem. B* **1998**, *102*, 3586.
- (49) Mackerell, A. D.; Feig, M.; III, C. L. B. *J. Comput. Chem.* **2004**, *25*, 1400.
- (50) Chen, C.-Y.; Ko, T.-P.; Lin, T.-W.; Chou, C.-C.; Chen, C.-J.; Wang, A. H.-J. *Nucleic Acids Res.* **2005**, *33*, 430.
- (51) Gao, Y.; Su, S.; Robinson, H.; Padmanabhan, S.; Lim, L.; McCrary, B.; Edmondson, S.; Shriner, J.; Wang, A. *Nat. Struct. Mol. Biol.* **1998**, *5*, 782.
- (52) Jorgensen, W. L.; Chandrasekhar, J.; Madura, J. D.; Impey, R. W.; Klein, M. L. *J. Chem. Phys.* **1983**, *79*, 926.

- (53) Field, M. J.; Karplus, M. *CRYSTAL: Program for Crystal Calculations in CHARMM*; Harvard University: Cambridge, MA, 1992.
- (54) Essmann, U.; Perera, L.; Berkowitz, M.; Darden, T.; Lee, H.; Pedersen, L. *J. Chem. Phys.* **1995**, *103*, 8577.
- (55) Ryckaert, J.-P.; Ciccotti, G.; Berendsen, H. J. C. *J. Comp. Phys.* **1977**, *23*, 327.
- (56) Hoover, W. G. *Phy. Rev.* **1985**, *A 31*, 1695.
- (57) Feller, S. E.; Zhang, Y.; Pastor, R. W.; Brooks, R. W. *J. Chem. Phys.* **1995**, *103*, 4613.
- (58) Humphrey, W.; Dalke, A.; Schulten, K. *J. Mol. Graph* **1996**, *14*, 33.
- (59) Frishman, D.; Argos, P. *Proteins: Struct., Funct., Genet.* **1995**, *23*, 566.
- (60) Knapp, S.; Karshikoff, A.; Berndt, K.; Christova, P.; Atanasov, B.; Ladenstein, R. *J. Mol. Biol.* **1996**, *264*, 1132.
- (61) Shehi, E.; Serina, S.; Fumagalli, G.; Vanoni, M.; Consonni, R.; Zetta, L.; DehU, G.; Tortora, P.; Fusi, P. *FEBS Lett.* **2001**, *497*, 131.
- (62) Wolf-Watz, M.; Thai, V.; Henzler-Wildman, K.; Hadjipavlou, G.; Eisenmesser, E.; Kern, D. *Nat. Struct. Mol. Biol.* **2004**, *11*, 945.
- (63) Henzler-Wildman, K.; Thai, V.; Lei, M.; Ott, M.; Wolf-Watz, M.; Fenn, T. *Nature* **2007**, *450*, 838.
- (64) Liang, Z.; Lee, T.; Resing, K.; Ahn, N.; Klinman, J. *Proc. Natl. Acad. Sci.* **2004**, *101*, 9556.
- (65) Liang, Z.-X.; Tsigos, I.; Lee, T.; Bouriotis, V.; Resing, K. A.; Ahn, N. G.; Klinman, J. P. *Biochemistry* **2004**, *43*, 14676.
- (66) Maiti, R.; Van Domselaar, G.; Zhang, H.; Wishart, D. *Nucleic Acids Res.* **2004**, *32*, W590.

JP909122X